ISSN 2411-3336; e-ISSN 2541-9404

JOURNAL OF MINING INSTITUTE
Zapiski Gornogo instituta
Journal homepage: pmi.spmi.ru

Research article
UDC 549.08

Rapid detection of coal ash based on machine learning and X-ray fluorescence

JINZHAN HUANG, ZHIQIANG LI, BIAO CHEN, SEN CUI, ZHAOLIN LU, WEI DAI, YUEMIN ZHAO, CHENLONG DUAN, LIANG DONG ✉
China University of Mining & Technology, Xuzhou, China

How to cite this article: Jinzhan Huang, Zhiqiang Li, Biao Chen, Sen Cui, Zhaolin Lu, Wei Dai, Yuemin Zhao, Chenlong Duan, Liang Dong. Rapid detection of coal ash based on machine learning and X-ray fluorescence. Journal of Mining Institute. 2022. Vol. 256, p. 663-676. DOI: 10.31897/PMI.2022.89

Abstract. Real-time testing of coal ash plays a vital role in the chemical, power generation, metallurgical, and coal separation sectors. The rapid online testing of coal ash using radiation measurement as the mainstream technology has problems such as strict coal sample requirements, poor radiation safety, low accuracy, and complicated equipment replacement. In this study, an intelligent detection technique based on feed-forward neural networks and improved particle swarm optimization (IPSO-FNN) is proposed to predict coal quality ash content in a fast, accurate, safe, and convenient manner. The data set was obtained by testing the elemental content of 198 coal samples with X-ray fluorescence (XRF). The types of input elements for machine learning (Si, Al, Fe, K, Ca, Mg, Ti, Zn, Na, P) were determined by combining the X-ray photoelectron spectroscopy (XPS) data with the change in the physical phase of each element in the coal samples during combustion. The mean squared error and coefficient of determination were chosen as the performance measures for the model. The results show that the IPSO algorithm is useful in adjusting the optimal number of nodes in the hidden layer. The IPSO-FNN model has strong prediction ability and good accuracy in coal ash prediction. The effect of the input element content of the IPSO-FNN model on the ash content was investigated, and it was found that the potassium content was the most significant factor affecting the ash content. This study is essential for real-time online, accurate, and fast prediction of coal ash.

***Keywords*:** ash prediction; elemental content; feed-forward neural networks; improved particle swarm optimization; principal component analysis

Acknowledgment. The authors acknowledge the financial support by the Natural Science Foundation of Jiangsu Province (N BK20200087) and the National Natural Science Foundation of China (N 51620105001).

Received: 13.05.2022 ***Accepted: 24.09.2022*** ***Online: 03.11.2022*** ***Published: 03.11.2022***

Introduction. Coal energy is widely used in the chemical industry, power generation, and metallurgy and still plays an irreplaceable role even in the new situation of energy diversification [1, 2]. China is the world's largest producer and consumer of coal, produced 4.13 billion tons of raw coal in 2021, up 5.7 percent from 2020 [3]. Energy consumption totaled 5.24 billion tons of standard coal, an increase of 5.2 percent over 2020, and coal consumption increased by 4.6 percent [3]. Coal consumption accounts for 56.0 percent of total energy consumption. The coal-based energy structure has supported China's rapid economic development.

Coal is made up of combustible organic matter and non-combustible minerals [4]. Coal ash refers to the solid waste produced by the decomposition and chemistry of the minerals in coal after it has been entirely burned under certain conditionsc [5]. High ash content in coal increases the resistance to heat and mass transfer during combustion and reduces combustion efficiency [6], especially in the middle and late coal combustion stages [7, 8]. In addition to this, possible corrosion, fouling and slagging problems in the combustion and gasification of coal can be predicted based on the ash

content. The ash content of the coal is also an auxiliary indicator for the valuation of power coal by calorific value.

To date, the standard method for determining the ash content of coal is still the scorch weighing method. The traditional method of burning and testing coal ash is complicated. The measurement process takes about 90 min [9], giving long lag time results, which can no longer meet modern coal processing and utilization enterprises' needs to produce coal for rapid ash measurement and online testing efficiently.

Currently, the mainstream techniques for rapid online detection of coal ash include natural radioactivity methods [10], weighing, photoelectric ash measurement [11], image processing ash measurement, and radiometric methods. Of these, the low-energy γ-ray backscatter method requires strict coal and geometric conditions to be measured, making it difficult to achieve online measurements. The high-energy gamma rays have a strong penetrating ability, rugged shielding, and poor radiation safety. Natural gamma radioactivity measurements of coal ash are susceptible to environmental background radiation and are more challenging to measure accurately. The dual-energy γ-ray transmission method is sensitive to the elemental composition and content of the coal. It can be affected by fluctuations in the content of high atomic number elements in the coal. Due to its short half-life, frequent replacement of radioactive sources is costly and complicated.

Artificial neural networks (ANN) have the potential to rely on faster, more accurate, and more practical characteristics as an alternative method for predicting coal burning behavior. Unfortunately, there are few studies on the effect of ANN on ash content. D.Ali [12] uses ANN in the flotation process to predict the ash content of coal based on polymer dosage, pH value, polymer conditioning time, sodium metasilicate dosage (commercial dispersant) and impeller velocity. P.Ilamathi [13] studied the influence of excess air, coal quality, boiler load, air distribution scheme and nozzle tilt on boiler bottom ash through ANN-GA. Based on the element content of coal, this study combined improved particle swarm optimization and feedforward neural network (IPSO-FNN) to predict ash quickly and accurately. The prediction of ash content not only determines the value of coal, but also has a deeper influence on the cleaning process.

With the development of statistics, machine learning algorithms, and spectral analysis instruments, research on the application of spectral analysis techniques in coal quality analysis is gradually gaining attention. The X-ray fluorescence (XRF) technique [14-16] and spectroscopy methods [17-19] are often used separately to determine ash composition, they are also relatively convenient method [20]. F.J.Wallis et al. [21] and J.M.Andrés et al. [22] used spectral detection techniques to analyze and predict the significant elements in coal and coal ash, respectively, with high prediction accuracy and correlation. M.Kaihara et al. [23] used spectral analysis techniques to predict the main properties of coal with high accuracy of the final prediction results.

Spectral analysis techniques with their unique advantages have been better studied and integrated into coal and chemical applications, showing their potential for predictive applications and good robustness. Feed-forward neural networks [24] have been used in many fields [25-27] as mathematical models with simple principles and high computational accuracy in machine learning [28].

W.Dai et al. [29] used a machine learning model to develop an acceptable coal ash model based on a variable block width incremental random configuration network and proposed an online adaptive semi-supervised learning based proper coal ash model [30]. Machine learning tools have been shown to have the ability to provide data-driven mechanical understanding and models [31], with good predictive potential [32] and robustness [33]. W.Liang et al. [28] and M.Srishti et al. [34] developed a model for predicting the ash content of the characteristic melt temperature and ignition characteristics three-layer neural network model. They found that their predictions were more accurate.

D.Durgun [35] studied the influence of coal properties on the yield of solid residue during combustion, investigated the correlation between bottom ash yield, ash content, moisture and calorific

value of coal combustion, and drew the conclusion that calorific value was the most critical factor affecting low ash yield. On the basis of previous work, Tugce [36] uses a three-layer feedforward network architecture and backpropagation learning to predict the amount of bottom ash generated in the process of coal burning in power plants based on the water content, ash content and low calorific value of coal. When the model is a single hidden layer network containing 29 neurons, the best performance is obtained.

I.Siregar [37] estimated ash content based on fuzzy curve and integrated neural network according to the composition of six major oxides, which effectively reduced the variance and bias of prediction and obtained better prediction results. In addition to coal quality evaluation, artificial neural network technology has also been applied in gas-solid fluidized bed medium small bubble diameter prediction [38], circulating fluidized bed riser flow prediction [32], estimation of cleaned coal ash in flotation process [39]. At the same time, Xu [40] added Pearson correlation coefficient (PCA) and other statistical methods to the nonlinear regression process, which reduced the number of variables in the analysis process, improved the prediction accuracy of the model, and prevented the risk of over-fitting and the waste of data sets.

In this context, to better utilize coal resources efficiently and cleanly, this paper proposes a new technology for real-time online rapid detection of coal ash based on the combination of machine learning and X-ray fluorescence.

An intelligent detection technique based on feed-forward neural networks and improved particle swarm optimization is proposed to predict coal samples' ash content quickly, accurately, safely, and conveniently. Feedforward neural network algorithm is used to model the nonlinear relationship between input and output, and improved particle swarm optimization algorithm is used to optimize the optimal solution number combination of hidden layer, so as to obtain better generalization ability and convergence ability of the model. Through XRF and XPS tests, the composition of various elements of coal samples and the phase changes of each element when coal samples are fully burned are studied, and the occurrence state and relative content of each element in coal samples are analyzed, so as to determine the element input of FNN-IPSO model.

Principal component analysis (PCA) and Pearson correlation coefficient analysis (PCC) were used to study and analyze the importance and correlation of each input variable, and the influence order of each element on ash content was obtained.

The main purpose of this paper is to study the influence of various elements content in coal on coal ash in order to realize the online detection task of coal ash. The results show that the IPSO-FNN model has high accuracy and can be used in the online detection of coal quality in coal preparation industry. This study is a pioneering work on applying improved particle swarm optimization and feedforward neural network (IPSO-FNN) jointly in coal ash prediction, which is vital for real-time online, accurate, and fast prediction coal ash.

Methods. ***Experimental tests.*** A series of experimental tests were conducted to provide a dataset for machine learning. The coal samples used in this experiment were taken from coal seams 7, 9, 11 and 12 of Heishan opencast coal mine in Xinjiang, China. The total thickness of the coal-bearing strata in the opencast mine is 506-1200 m. The coal seam is mainly quartzite, slime, sandstone, mudstone and shale. Xinjiang Heishan opencast mine is located in Tokxun County, Turpan region, Xinjiang Province. Its raw coal clean grade is two, which can be used as high quality steam coal. In each seam, clean coal, medium coal and gangue of different particle sizes are collected sequentially as analytical coal samples. In order to ensure that the coal sample is representative, different parts of each coal seam are sampled and mixed evenly by using the quartile method. The coal samples were crushed, sieved, reduced, mixed and air dried according to the test standards GB 475-2008, GB T 477-2008 and GB T 478-2008 to produce the base coal samples for this test.

To further analyze the coal quality characteristics and elemental composition of the coal samples, the elemental composition and content of 198 sets of coal samples were obtained by XRF testing. Next, based on the X-ray photoelectron spectroscopy (XPS) data and combined with each element's physical phase changes in the coal sample during combustion, each element's form and relative content of the coal sample are analyzed. Then the input element types for machine learning are determined. In general, quantitative analysis and element morphology analysis in coal samples are achieved by XRF and XPS tests. In this study, S8-Tiger fluorescence spectrometer was used to analyze the elemental composition of coal samples, and the current reached 170 mA to achieve good excitation. An ESCALAB 250Xi X-ray photoelectron spectrometer was used to analyze the occurrence forms of elements in coal samples. The detection energy range was 0-5000 eV, and the resolution of photoelectron images was up to 3 μm.

As the coal samples provided in the data set come from different coal seams with different grain sizes and density levels, the experimental data are unstable and fluctuate greatly. Random shuffle and segmentation of the data set can reduce the error caused by human. In this experiment, the data set is divided into training set (85 %) and test set (15 %). The training set is used to train the model, and the test set is used to test the model performance.

Feed-forward neural networks. Feed-forward Neural Network (FNN) is the first simple artificial neural network to be invented. In the FNN, each neuron belongs to a different layer. The neurons in each layer can receive signals from the previous layer's neurons and produce output signals to the next layer. The zeroth layer is called the input layer, the last layer is called the output layer, and the other intermediate layers are called the hidden layers. Feed-forward neural networks propagate information by continuously iterating the following equation:

$$Z^{(l)} = W^{(l)} a^{(l-1)} + b^{(l)}; \tag{1}$$

$$a^{(l)} = f_l(z^{(l)}), \tag{2}$$

where l is the number of layers of the neural network; $Z^{(l)}$ is the input of the neuron at layer l; $W^{(l)}$ is the weight matrix from layer $l-1$ to layer l; $f_l(z^{(l)})$ is the activation function of the neuron at layer l; $a^{(l)}$ is the output of the neuron at layer l; $b^{(l)}$ is the bias from layer $l-1$ to layer l.

Due to its strong fitting capability, FNN can be used to approximate standard continuous nonlinear functions. Kolmogorov's [41] theorem states that any ongoing process can be implemented precisely with a three-layer FNN. However, based on experience and continuous experimentation, for non-linear functions of moderate complexity, a four-layer neural network requires far fewer neurons to simulate and converges much faster than a three-layer neural network. Therefore, the FNN model with two hidden layers is chosen to predict coal samples' ash content in this paper. The software used in this experiment to establish the neural network model is Python 3.9. Compared with C language, Python is more in line with the logic of human thinking and the code is simpler. Scikit-learn is a machine learning library for Python 3.9 programming language, which contains modules for data preprocessing, dataset partitioning, model optimization and other works. This will greatly reduce the workload of the experiment.

Improved particle swarm optimization. To develop an integrated model with superior performance, it is essential to determine the optimal number of node combinations in the hidden layer after determining the network structure layers. Optimization technology is a mathematical-based application technique for solving various engineering problems optimally. Particle swarm optimization (PSO) is an algorithm for population intelligence optimization that requires fewer parameters to be adjusted, which has a simple structure and is easy to implement in engineering. The particle position update formula used in this paper is as follows:

$$V_{id}^{k+1} = \omega V_{id}^{k} + c_1 r_1 (P_{id}^{k} - X_{id}^{k}) + c_2 r_2 (P_{gd}^{k} - X_{id}^{k}); \quad (3)$$

$$X_{id}^{k+1} = X_{id}^{k} + v_{id}^{k+1}, \quad (4)$$

where V_{id}^{k+1}, V_{id}^{k} denote the velocity of the particle at iteration $k + 1$ and k; X_{id}^{k+1}, X_{id}^{k} denote the position of the particle at iteration $k + 1$ and k; P_{id}^{k}, P_{gd}^{k} denote the best position of the particle and the best position of the swarm, which will be updated at each iteration using the target MSE; ω denotes the inertia factor; k denotes the number of current iterations; c_1, c_2 are non-negative constants denoting the learning factor; r_1, r_2 are random numbers between 0, 1; $d = 1,2 \ldots D$; $i = 1,2 \ldots n$.

Improving the particle swarm optimization is to set the parameters of certain factors appropriately in the solution process. The parameters in the classical PSO algorithm are determined empirically. However, in this paper, the inertia factor is adjusted by an adaptive method:

$$\omega = (\omega_{\max} - \omega_{\min}) \frac{k_{\max} - k}{k_{\max}} + \omega_{\min}, \quad (5)$$

where $\omega_{\min}$, $\omega_{\max}$ denote the minimum and maximum value of the inertia factor ω respectively; $k_{\max}$ denotes the full value of the number of iterations.

This equation can satisfy the requirement of a large inertia factor required in the search's early stages. Subsequently, the inertia factor can be reduced appropriately to satisfy local search capability requirement as far as possible. The value of ω can be decreased during the search process.

During the iterative search process, the learning factor can be made to vary appropriately with the inertia factor, which helps to improve the learning performance of the algorithm, resulting in the following expression:

$$c_1 = c_{1\max} - (c_{1\max} - c_{1\min}) \cos(\omega); \quad (6)$$

$$c_2 = c_{2\max} - (c_{2\max} - c_{2\min}) \cos(\omega), \quad (7)$$

where $c_{1\min}$, $c_{1\max}$ denote the optimal value of learning factor c_1, respectively; $c_{2\min}$, $c_{2\max}$ denote the optimal value of learning factor c_2, respectively.

With the use of the learning factor algorithm for analysis, its ability to self-learn can be improved, while facilitating improved search accuracy.

IPSO-FNN modelling. To train an FNN using the improved particle swarm optimization, a suitable objective function is required. As the mean squared error (MSE) is often used as a loss function in FNN, it can be used as an adaptation function in the IPSO-FNN integrated model. The mean square error is defined as:

$$\mathrm{MSE} = \frac{1}{N} \sum_{i=1}^{N} (y_i^* - y_i)^2, \quad (8)$$

where N is the number of sample data; y_i^*, y_i are the predicted and tested values of the sample, respectively.

The IPSO-FNN integrated model in this paper combines the advantages of improved particle swarm optimization and feed-forward neural networks. IPSO is used to find the optimal number of node combinations for the two hidden layers, and FNN is used to predict the best result for the ash content of the coal samples. The entire dataset is divided into two parts: the training set (85 %) and the test set (15 %). Based on adjustment experience, the number of nodes in the two hidden layers is adjusted in the range of 10-40. From the literature [42], the population size and the maximum number of iterations were 20 and 300, respectively. In the paper, the inertia factor is adjusted by (5), and then

Journal of Mining Institute. 2022. Vol. 256. P. 663-676 DOI: 10.31897/PMI.2022.89

the learning factor is adjusted appropriately by (6) and (7) according to the change in the inertia factor. The flow chart of the IPSO optimized hidden layer network node algorithm is shown in Fig.1.

Results discussion. ***Results of tests.*** From Fig.2, *a*, it can be seen that the range of variation and dispersion of the distribution of ash values of different components of coal samples are extensive, and the ash content of coal samples is high, which belongs to high ash~extra high ash coal. Fig.2, *b* shows the variation of ash data in the range of 1.44 to 94.1, where there are 50 groups with ash values from 1.44 to 20, 80 groups with ash values from 20 to 60, and 60 groups with ash values from 60 to 94.1. It can be seen that the coal samples have high extreme differences in ash values, which is challenging for the robustness of the prediction model.

XRF tests were performed on 198 coal samples, respectively, and one group (89 groups) of the test results are shown in Table 1. The content of each element in the coal sample varies greatly, and the significant elements are Si, Al, Fe, S, K, Ca, Mg, Ti, Cl, Zn, Na, P, Ba, V, Cu, Sr, Mn, Cr, Zr, Ru,

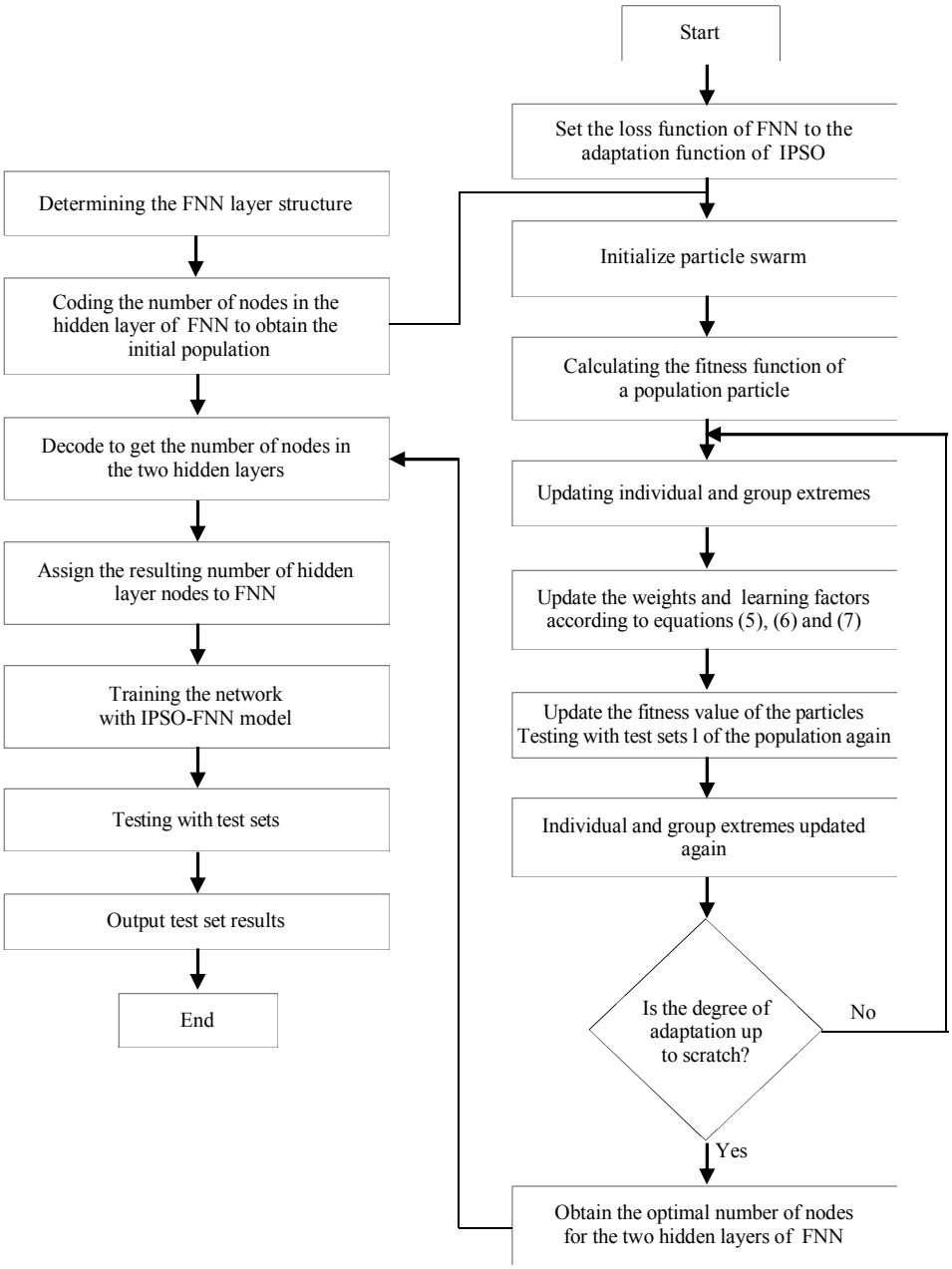

Fig.1. IPSO optimized hidden layer network node flow chart

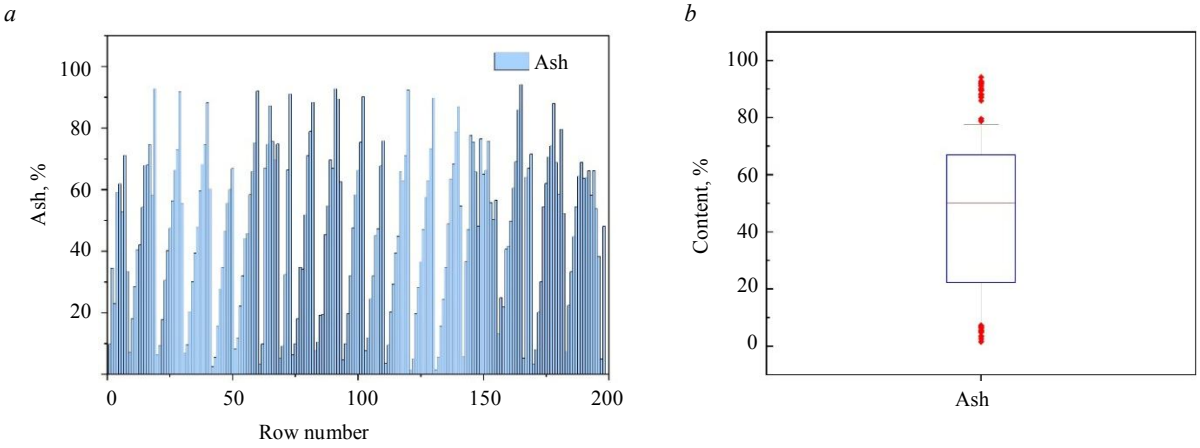

Fig.2. Ash test results of coal samples: *a* – actual input values; *b* – statistical distribution

Ni, Rb, as in descending order. From the content of each element in Table 1, it can be seen that the main elements in the coal samples are Si and Al, followed by Fe, S, K, etc. Among them, the content of Si and Al elements exceeds 50 %, the content of Fe, S, K, Ca, Mg, Ti, Ch, Zn, Na, P, and Ba are more significant than 0.05 %, and the content of all other elements varies within the range of less than 0.05 %. This results in negligible elemental content of V, Cu, Sr, Mn, Cr, Zr, Ru, Ni, Rb, and As.

Table 1

XRF test results of group 89 coal samples

Molecular formula	Atomic mass of an element	Content, %
SiO_2	14	34.63
Al_2O_3	13	15.47
Fe_2O_3	26	2.92
SO_3	16	2.44
K_2O	19	1.13
CaO	20	0.984
MgO	12	0.923
TiO_2	22	0.644
Cl	17	0.5
ZnO	30	0.4252
Na_2O	11	0.308
P_2O_5	15	0.065
BaO	56	0.054
V_2O_5	23	0.021
CuO	29	0.0152
SrO	38	0.0145
MnO	25	0.012
Cr_2O_3	24	0.008
ZrO_3	40	0.0063
Ru	44	0.006
NiO	28	0.005
Rb_2O	37	0.003
As_2O_3	33	0.003

Each element's fugitive state in the coal sample is changed after the ash burn test is performed. Since the XRF test can only yield each central element's content in the coal sample, it cannot determine the form of each element present in the coal sample before ash burning. Therefore, XPS tests are needed to determine the condition and relative content of each element present in the coal sample and combine each element's physical phase changes in the coal sample during combustion to determine

Journal of Mining Institute. 2022. Vol. 256. P. 663-676 DOI: 10.31897/PMI.2022.89

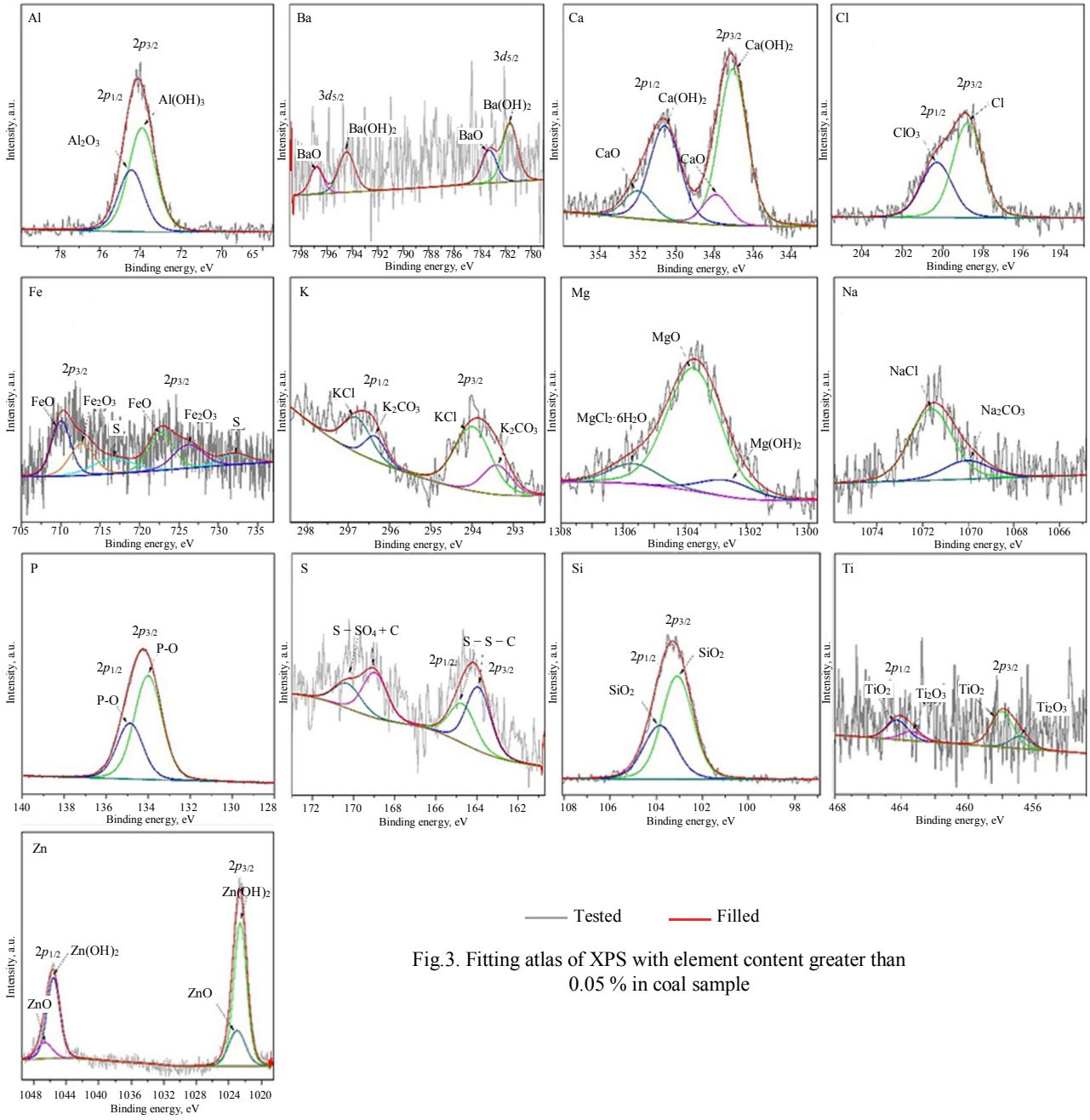

Fig.3. Fitting atlas of XPS with element content greater than 0.05 % in coal sample

the types of input elements for the machine learning finally. Fig.3 shows the fitted XPS spectra of the coal samples with each element's more significant than 0.05 % content. The peaks of each element's binding energy (content greater than 0.05 %) attributed to the group (a form of presence), relative content, and physical phase change are shown in Table 2.

Table 2

Changes in the physical phase of elements with content greater than 0.05 %

Element type	Forms of presence	Relative content	Change of physical phase	Decisions
Ca	$Ca(OH)_2$ CaO	82.14 17.86	$Ca(OH)_2 \rightarrow CaO + H_2O$ No change	Reserved
Si	Si_2O	100	$Si_2O + FeO \rightarrow FeO{\cdot}Si_2O$	Reserved
S	S_{org} S_{inorg}	59.07 40.93	$S + O_2 \rightarrow SO_2$ $CaSO_4{\cdot}2H_2O \rightarrow CaSO_4 + 2H_2O$	Removal

End of Table 2

Element type	Forms of presence	Relative content	Change of physical phase	Element type
Fe	FeO Fe_2O_3	45.02 33.76	$FeO + SiO_2 \rightarrow FeO{\cdot}SiO_2$ No change	Reserved
Al	$Al(OH)_3$ Al_2O_3	64.13 35.87	$2Al(OH)_3 \rightarrow Al_2O_3 + 3H_2O$ $Al_2O_3 + 3SiO_2 \rightarrow Al_2O_3{\cdot}3SiO_2$	Reserved
Mg	MgO $MgCl_2{\cdot}6H_2O$ $Mg(OH)_2$	77.93 11.69 10.38	No change $MgCl_2{\cdot}6H_2O \rightarrow MgO + 2HCl + 5H_2O$ $Mg(OH)_2 \rightarrow MgO + H_2O$	Reserved
Cl	Cl^- Cl_3^-	62.10 37.90	No change $2Cl_3^- \rightarrow 2Cl^- + 3O_2$	Removal
Zn	$Zn(OH)_2$ ZnO	77.77 22.23	$Zn(OH)_2 \rightarrow ZnO + H_2O$ No change	Reserved
Na	NaCl Na_2CO_3	78.04 21.96	No change $Na_2CO_3 \rightarrow Na_2O{\cdot}CO_2$	Reserved
K	KCl K_2CO_3	70.80 29.20	No change $K_2CO_3 \rightarrow K_2O + CO_2$	Reserved
P	HPO_3	100	$P_2O_3 + 3H_2O \rightarrow 2H_3PO_4$ $H_3PO_4 \rightarrow HPO_3 + H_2O$	Reserved
Ti	TiO_2 Ti_2O_3	73.25 26.75	No change No change	Reserved
Ba	$Ba(OH)_2$ BaO	63.97 36.03	$Ba(OH)_2 \rightarrow BaO + H_2O$ No change	Removal

As can be seen from Table 2, organic sulfur and inorganic sulfur are the primary forms of elemental sulfur in coal samples, with relative contents of 59.07 and 40.93 %, respectively. During the thermal evolution of slow ashing of coal samples, organic sulfur is volatilized as gas, and inorganic sulfur is present in the ash of coal samples as sulfate. The coal samples' elemental chlorine existed mainly in chlorate and hypochlorite forms, with relative contents of 62.1 and 37.90 %, respectively. Hypochlorite is converted to chlorate as the slow ashing progresses, while chlorate is released in gas or soot. The magnesium in the coal samples was mainly in magnesium oxide, chlorite, and magnesium hydroxide. Chlorite is converted to magnesium hydroxide, converted to magnesium oxide present in the coal sample's ash. The potassium and sodium elements in the coal samples are present in the fugitive forms of chloride and carbonate. During the thermal evolution of slow ashing, the potassium and sodium elements' carbonate phases are transformed into potassium oxide and sodium oxide, respectively, in the coal samples' ash. Ca, Si, Fe, Al, Zn, P, Ti, and Ba are present in the fugitive forms of oxides and hydroxides in the coal samples. During the thermal evolution of slow ashing, most of the hydroxides are converted to oxides and are all present as oxides in the coal sample's ash.

Analysis of the form and relative content of the elements present in the above coal samples by XPS shows that most of the sulfur and chlorine elements in the coal samples are released in the form of gas or soot during the thermal evolution of the burnt ash and are not present in the ash of the coal samples [43]. In contrast, the elements Si, Al, Fe, K, Ca, Mg, Ti, Zn, Na, P, and Ba are retained in the ash of the coal sample in the form of oxides during the thermal evolution of the burnt ash [28]. This shows that a coal sample's ash content is closely related to the content of elements such as Si, Al, Fe, K, Ca, Mg, Ti, Zn, Na, P, and Ba. Also, according to XRF results, barium was not detected in 28 groups of 198 coal samples. Therefore, the elemental content of IPSO-FNN was entered in the order of Si, Al, Fe, K, Ca, Mg, Ti, Zn, Na, and P. The statistical distribution of the above ten elements is shown in Table 3 and the corresponding ash data are shown in Fig.2, *a*.

Journal of Mining Institute. 2022. Vol. 256. P. 663-676 DOI: 10.31897/PMI.2022.89

Results of architecture-tuning. Figure 4 shows the FNN minimum loss function (population best position) versus iteration for the first fifteen iterations using a combination of different numbers of nodes in the two hidden layers, with no further reduction in the minimum loss function after the fifteenth iteration. After the first iteration, the FNN minimum loss function dropped significantly, indicating that IPSO was useful in finding the optimal number of node combinations in the two hidden layers. The minimum loss function (0.095) was obtained at the fifteenth iteration (30 neurons in the first hidden layer and 30 neurons in the second hidden layer). The optimal FNN structure used to predict further the ash content of the coal sample is shown in Fig.5.

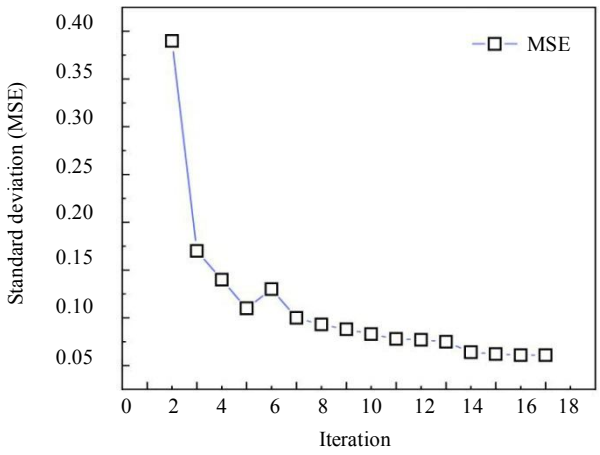

Fig.4. Mean squared loss function versus the number of iterations

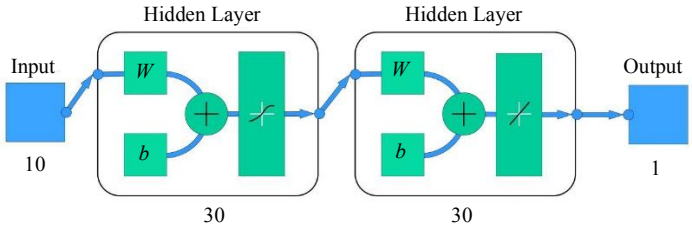

Fig.5. Schematic representation of the optimal FNN structure

Based on IPSO to obtain the optimal combination of the number of nodes in the two hidden layers, the FNN is trained with the training set to get the appropriate weights and biases. Then, the optimal FNN is constructed. The FNN model's performance was evaluated on the training and test sets using mean squared error and determination coefficient. The coefficient of determination, also known as the goodness of fit, is used to evaluate fit's goodness. The coefficient of determination is defined as

$$R^2 = 1 - \frac{\sum (y_i^* - y_i)^2}{\sum (y_i^{**} - y_i)^2}, \quad (9)$$

where y_i^{**} – is the mean of the tested values.

A higher coefficient of determination means that it can be explained to a greater extent and the regression model is more effective.

Results of the optimum FNN model. A comparison of the experimental and predicted values of the IPSO-FNN model on the test set is shown in Fig.6, *a*. It can be seen that the IPSO-FNN model with the optimum number of node combinations in the two hidden layers successfully simulates the non-linear relationship between the elemental content of Si, Al, Fe, K, Ca, Mg, Ti, Zn, Na, and P and the ash content in the coal samples. Fig.6, *b* shows that the optimal IPSO-FNN model obtained a minimum loss function of 0.019 and a coefficient of determination of 0.091 on the test sets. It can be seen that the optimal IPSO-FNN model can be generalized to the test set with high accuracy, indicating that the optimal IPSO-FNNN model is more accurate in predicting the ash content of coal samples.

Principal component analysis of elemental content. To better understand the influence of the input elemental content of the optimal IPSO-FNN model on the ash content and to explore the relative importance of the input elemental content and the correlation between the input variables, principal component analysis (PCA) and Pearson correlation coefficient analysis were performed on the input elemental content of the optimal IPSO-FNN model. The elemental content of coal can overlap information to a certain extent, making it difficult to grasp the main parts of its system while affecting the complexity of problem-solving. In addition to this, in practice, an excessive amount of data takes

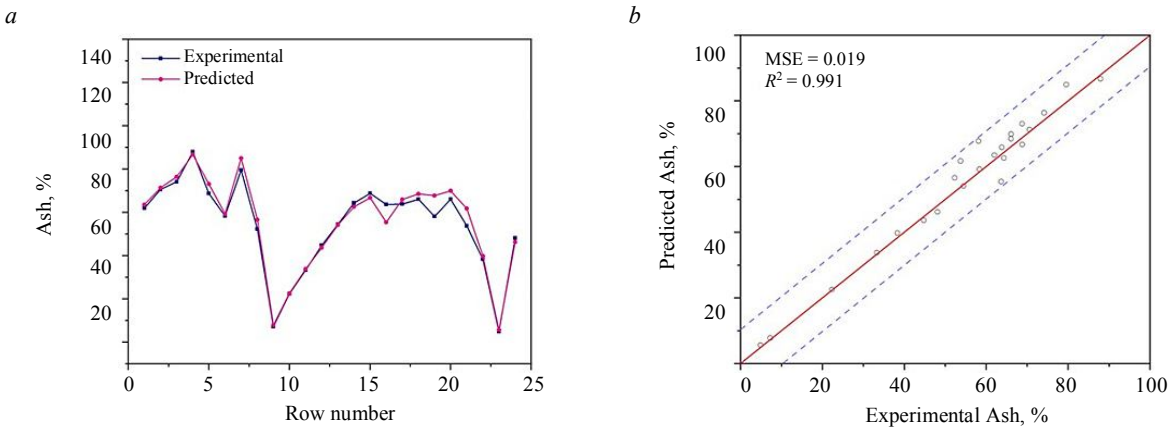

Fig.6. Performance of the optimal IPSO-FNN model on test sets: *a* – comparison of experimental and predicted values in test set; *b* – regression analyisis of test set

up a lot of storage space and increases the time taken to process the information. PCA is a feature extraction method based on the minimum mean square error under statistical significance [44]. The new features it extracts maintain most essential information in the original pattern class, achieving noise reduction and improving the data's representation. The effect of the input element content of the optimal IPSO-FNN model on the ash content was investigated by principal component analysis and matrix heat map of Pearson correlation coefficients.

The principal component analysis of the input element content of the optimal IPSO-FNN model is shown in Fig.7, *a*. The first principal component explains 59.6 % of the overall data variance, and the first five principal components explain 95.4 % of the conflict. The correlation between the first five principal components and elemental content is shown in Fig.7, *b*. The correlations of K, Si, Al, Ti, and Mg with the first principal component are 0.95, 0.94, 0.93, 0.92, and 0.8, respectively. The potassium content contributed most to the first principal component, and the content of calcium contributed least to the first principal component.

The statistical distribution of the content of ten elements of the optimal IPSO-FNN model was obtained Table 3, as can be seen from Table 3, Si and Al are the main components of the relative elemental coal content. the dispersion degree of ash is the largest, and its standard deviation reaches 26.26, followed by Si and Al, which are 16.59 and 6.95, respectively. The rest of the elements have less dispersion degree and more stable. Combining Fig.7, *b* and Table. 3 shows that elements with a relatively high content (Si, Al, Fe, Ca, Na) do not significantly affect ash than parts with relatively low content (K, Ti, Mg, Zn). However, the content of phosphorus is positively correlated with the pattern of effect on ash.

Table 3

Statistical analysis of input and output element content of optimal IPSO-FNN model

Variables	Maximum	Minimum	Average	Standard deviation
Si	56.33	0.94	27.13	16.59
Al	23.99	0.66	12.26	6.95
Fe	8.86	0.85	3.43	1.35
Ca	17.94	0.22	2.96	2.76
K	3.05	0.03	1.33	0.90
Mg	2.22	0.18	1.00	0.50
Ti	0.88	0.02	0.45	0.25
Zn	6.22	0.03	0.91	1.14
Na	2.76	0.08	0.44	0.35
P	0.72	0.01	0.10	0.09
Ash	94.10	1.44	46.88	26.26

Journal of Mining Institute. 2022. Vol. 256. P. 663-676 DOI: 10.31897/PMI.2022.89

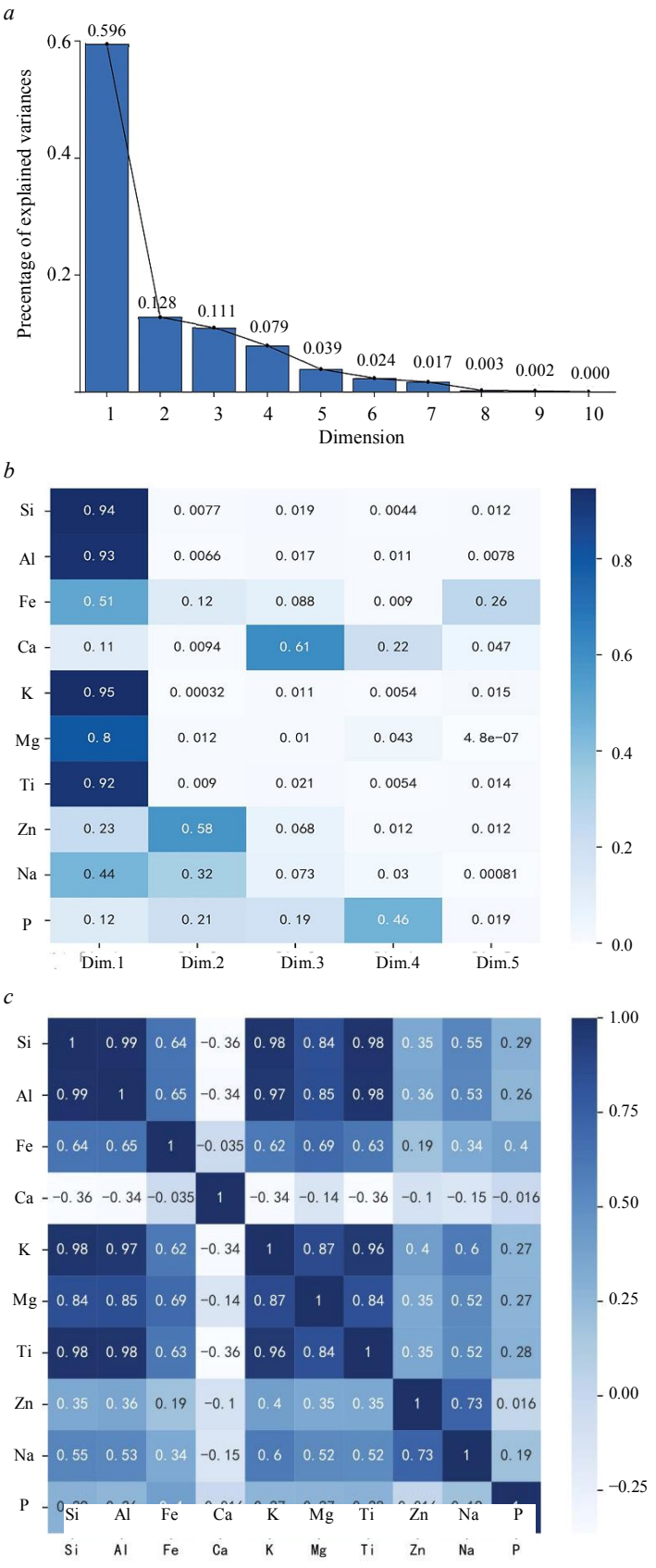

Fig.7. Principal component analysis of the input element content of the optimal IPSO-FNN model (*a*), heat maps of the correlation matrix between the input element content and the top five principal components (*b*) and correlation coefficient matrix for the input element content (*c*) of the optimal IPSO-FNN model

A Pearson correlation coefficient analysis was performed for each elemental content to analyze further the interrelationships between the input elemental contents of the optimal IPSO-FNN model, as shown in Fig.8. The larger the absolute value of the correlation coefficient, the more significant the correlation between the features. As can be seen from Fig.8, the content of potassium is positively correlated with the content of Si, Al, and Fe, with correlation coefficients of 0.98, 0.98, and 0.62, respectively. In contrast, it is negatively correlated with calcium content, with a correlation coefficient of −0.34. This phenomenon correlates with the low correlation (0.11) between the elemental calcium content and the first principal component in Fig.7, *a*. Simultaneously, the potassium content showed a positive correlation with the Ti, Mg, Na, and P content, with correlation coefficients of 0.96, 0.87, 0.6, 0.27, and 0.4, respectively. It can also be seen from Fig.8 that the content of calcium is negatively correlated with the content of all other elements. This phenomenon may be related to the form and transformation of calcium present in the ash burning process, and further research is needed to understand this point.

In summary, PCA and Pearson correlation coefficient matrix heat maps reveal significant findings and point to potentialresearch implications for the prediction of ash by elemental content.

Conclusions. In this study, an online fast prediction model for coal ash is proposed based on feed-forward neural networks and improved particle swarm optimization algorithms. Si, Al, Fe, K, Ca, Mg, Ti, Zn, Na, and P were identified as the FNN input elements, and the output was the ash. The performance of the IPSO-FNN model was verified through mean square error and coefficient of determination. The results show that the IPSO-FNN model has strong predictive power and good accuracy in coal ash prediction. The IPSO algorithm was useful in tuning the optimal number of node combinations in the hidden layer of the FNN model. The obtained optimal

IPSO-FNN model performed well on the test set, getting a minimum loss function of 0.019 and a coefficient of determination of 0.991 on the test set.

The correlation of the input element content of the optimal IPSO-FNN model was investigated. It was found that the first principal component could explain 59.6 % of the variation in the whole dataset. The most considerable contribution to the first principal component was the potassium content, with a correlation coefficient of 0.95. The matrix heat map of the Pearson correlation coefficient shows that the content of potassium is the most significant factor affecting the ash content. Si, Al, Ti, and Mg's content are the main factors affecting the ash content. This study serves as a pioneering work in the online prediction of coal ash, and the proposed IPSO-FNN model can be effectively applied in future industrial applications.

One thing to note, The coal samples were collected from coal seams 7, 9, 11 and 12 of Heishan open-pit mine in Xinjiang with different grain grades and density grades, therefore, the scope of this article is coal from these four coal seams. The correlation between the element content and ash content of coal in different geographical locations may be different, which will affect the prediction accuracy of the model. Collecting coal samples from other coal seams or regions to improve the model is the focus of the next work.

REFERENCES

1. Dong L., Zhao Y., Duan C. et al. Characteristics of bubble and fine coal separation using active pulsing air dense medium fluidized bed. *Powder Technology*. 2014. Vol. 257, p. 40-46. DOI: 10.1016/j.powtec.2014.02.049

2. Dong L., Zhou E., Cai L. et al. Fluidization characteristics of a pulsing dense-phase gas-solid fluidized bed for high-density separation of fine anthracite. *Energy & Fuels*. 2016. Vol. 30. Iss. 9, p. 7180-7186. DOI: 10.1021/acs.energyfuels.6b01468

3. Zhang Shengli, Tang Jiaxuan, Wang Meng. Challenges and opportunities for the development of China's coal industry under the background of carbon peak and carbon neutrality. *China Coal*. 2022. Vol. 48 (05), p. 1-5. DOI: 10.19880/j.cnki.ccm.2022.05.001

4. Levendisa Y.A., Joshia K., Khatamia R., Sarofim A.F. Combustion behavior in air of single particles from three different coal ranks and from sugarcane bagasse. *Combustion and Flame*. 2011. Vol. 158. Iss. 3, p. 452-465. DOI: 10.1016/j.combustflame.2010.09.007

5. Hai Feng Su, Furong Tan, Jia Fu Lin. An integrated approach combines hydrothermal chemical and biological treatment to enhance recycle of rare metals from coal fly ash. *Chemical Engineering Journal*. 2020. Vol. 395. N 124640. DOI: 10.1016/j.cej.2020.124640

6 Jayanti S., Maheswaran K., Saravanan V. Assessment of the effect of high ash content in pulverized coal combustion. *Applied Mathematical Modelling*. 2007. Vol. 31. Iss. 5, p. 934-953. DOI: 10.1016/j.apm.2006.03.022

7. Hurt R.H., Gibbins J.R. Residual carbon from pulverized coal fired boilers: 1. Size distribution and combustion reactivity. *Fuel*. Vol. 74. Iss. 4, p. 471-480. DOI: 10.1016/0016-2361(95)98348-I

8. Xu X., Chen Q., Fan H. The influence of high-temperature crystallite growth and petrography of pulverized char on combustion characteristics. *Fuel*. 2003. Vol. 82. Iss. 7, p. 853-88. DOI: 10.1016/S0016-2361(02)00380-0

9. Styszko-Grochowiak K., Gołaś J., Jankowski H., Koziński S. Characterization of the coal fly ash for the purpose of improvement of industrial on-line measurement of unburned carbon content. *Fuel*. 2004. Vol. 83. Iss. 13, p. 1847-1853. DOI: 10.1016/j.fuel.2004.03.005

10. Song W., Tang L., Zhu X. et al. Fusibility and flow properties of coal ash and slag. *Fuel*. 2008. Vol. 88. Iss. 2, p. 297-304. DOI: 10.1016/j.fuel.2008.09.015

11. Song W., Tang L., Zhu X. et al. Flow properties and rheology of slag from coal gasification. *Fuel*. 2009. Vol. 89. Iss. 7, p. 1709-1715. DOI: 10.1016/j.fuel.2009.07.013

12. Ali D., Hayat M.B., Alagha L., Molatlhegi O.K. An evaluation of machine learning and artificial intelligence models for predicting the flotation behavior of fine high-ash coal. *Advanced Powder Technology*. 2018. Vol. 29. Iss. 12, p. 3493-3506. DOI: 10.1016/j.apt.2018.09.032

13. Ilamathi P., Selladurai V., Balamurugan K. Modeling and Optimization of Unburned Carbon in Coal-Fired Boiler Using Artificial Neural Network and Genetic Algorithm. *Journal of Energy Resources Technology*. 2013. Vol. 135. Iss. 3. N 032201. DOI: 10.1115/1.4023328

14. Wang C., Zhao L., Yuan M. et al. Effects of ashing method and blending on ash characteristics of pyrolyzed and gasified semi-cokes. *Fuel*. 2020. Vol. 271. N 117607. DOI: 10.1016/j.fuel.2020.117607

15. Nguyen T.D., Nguyen A.V., Lin C.-L., Miller J.D. Application of high-resolution X-ray microcomputed tomography for coal washability analysis. *Minerals Engineering*. 2018. Vol. 124, p. 137-148. DOI: 10.1016/j.mineng.2018.05.027

16. Perring L., Tschopp A. Determination of ash content of milk-based powders by Energy Dispersive X-ray Fluorescence. *Microchemical Journal*. 2019. Vol. 145, p. 162-167. DOI: 10.1016/j.microc.2018.10.025

17. Li L., Wang C., Li W., Chen J. Hyperspectral image classification by AdaBoost weighted composite kernel extreme learning machines. *Neurocomputing*. 2018. Vol. 275, p. 1725-1733. DOI: 10.1016/j.neucom.2017.09.004

18. Gomez R.Y., Hernandez C.R., Guerrero E.J., Mejia-Ospino E. FTIR-PAS coupled to partial least squares for prediction of ash content, volatile matter, fixed carbon and calorific value of coal. *Fuel*. 2018. Vol. 226, p. 536-544. DOI: 10.1016/j.fuel.2018.04.040

19. Sheta S., Afgan M.S., Hou Z. et al. Coal analysis by laser-induced breakdown spectroscopy: a tutorial review. *Journal of Analytical Atomic Spectrometry*. 2019. Vol. 34. Iss. 6, p. 1047-1082. DOI: 10.1039/c9ja00016j

20. Xing P., Mason P.E., Chilton S. et al. A comparative assessment of biomass ash preparation methods using X-ray fluorescence and wet chemical analysis. *Fuel*. 2016. Vol. 182, p. 161-165. DOI: 10.1016/j.fuel.2016.05.081
21. Wallis F.J., Chadwick B.L., Morrison R.J.S. Analysis of Lignite Using Laser-Induced Breakdown Spectroscopy. *Applied Spectroscopy*. 2000. Vol. 54. Iss. 8. DOI: 10.1366/0003702001950814
22. Andrés J.M., Bona M.T. Analysis of coal by diffuse reflectance near-infrared spectroscopy. *Analytica Chimica Acta*. 2004. Vol. 535. Iss. 1-2, p. 123-132. DOI: 10.1016/j.aca.2004.12.007
23. Kaihara M., Takahashi T., Akazawa T. et al. Application of near infrared spectroscopy to rapid analysis of coals. *Spectroscopy Letters*. 2002. Vol. 35. Iss. 3. DOI: 10.1081/SL-120005673
24. Svozil D., Kvasnicka V., Pospichal J. Introduction to multi-layer feed-forward neural networks. *Chemometrics and Intelligent Laboratory Systems*. 1997. Vol. 39. Iss. 1, p. 43-62. DOI: 10.1016/S0169-7439(97)00061-0
25. Gayathri J.L., Abraham B., Sujarani M.S., Nair M.S. A computer-aided diagnosis system for the classification of COVID-19 and non-COVID-19 pneumonia on chest X-ray images by integrating CNN with sparse autoencoder and feed forward neural network. *Computers in Biology and Medicine*. 2022. Vol. 141. N 105134. DOI: 10.1016/j.compbiomed.2021.105134
26. Kolokythas K.V., Argiriou A.A. An application of a feed-forward neural network model for wind speed predictions. *International Journal of Sustainable Energy*. 2022. Vol. 41. Iss. 4, p. 323-340. DOI: 10.1080/14786451.2021.1915315
27. Bharath Y.K. Griffiths' Variable Learning Rate Online Sequential Learning Algorithm for Feed-Forward Neural Networks. *Automatic Control and Computer Sciences*. 2022. Vol. 56. Iss. 2, p. 160-165. DOI: 10.3103/S0146411622020031
28. Liang W., Wang G., Ning X. et al. Application of BP neural network to the prediction of coal ash melting characteristic temperature. *Fuel*. 2020. Vol. 260. N 116324. DOI: 10.1016/j.fuel.2019.116324
29. Dai W., Li D., Zhou P., Chai T. Stochastic configuration networks with block increments for data modeling in process industries. *Information Sciences*. 2019. Vol. 484, p. 367-386. DOI: 10.1016/j.ins.2019.01.062
30. Dai Wei, Hu Jin-Cheng, Cheng Yu-Hu et al. RVFLN-based online adaptive semi-supervised learning algorithm with application to product quality estimation of industrial processes. *Journal of Central South University*. 2019. Vol. 26. Iss. 12, p. 3338-3350. DOI: 10.1007/s11771-019-4257-6
31. Patel A.M., Cocco R.A., Chew J.W. Key influence of clusters of Geldart Group B particles in a circulating fluidized bed riser. *Chemical Engineering Journal*. 2020. Vol. 413. N 127386. DOI: 10.1016/j.cej.2020.127386
32. Chew J.W., Cocco R.A. Application of machine learning methods to understand and predict circulating fluidized bed riser flow characteristics. *Chemical Engineering Science*. 2020. Vol. 217. N 115503. DOI: 10.1016/j.ces.2020.115503
33. Pan J., Pottimurthy Y., Wang D. et al. Recurrent neural network based detection of faults caused byparticle attrition in chemical looping systems. *Powder Technology*. 2020. Vol. 367, p. 266-276. DOI: 10.1016/j.powtec.2020.03.038
34. Mittal S., Pathaka Sh., Dhawana H., Upadhyayula S. A machine learning approach to improve ignition properties of high-ash Indian coals by solvent extraction and coal blending. *Chemical Engineering Journal*. 2020. Vol. 413. N 127385. DOI: 10.1016/j.cej.2020.127385
35. Durgun D., Genc A. Effects of coal properties on the production rate of combustion solid residue. *Energy*. 2009. Vol. 34. Iss. 11, p. 1976-1979. DOI: 10.1016/j.energy.2009.08.005
36. Bekat T., Erdogan M., Inal F., Genc A. Prediction of the bottom ash formed in a coal-fired power plant using artificial neural networks. *Energy*. 2012. Vol. 45. Iss. 1, p. 882-887. DOI: 10.1016/j.energy.2012.06.075
37. Siregar I., Niu Y.F., Mostaghimi P., Armstrong R.T. Coal ash content estimation using fuzzy curves and ensemble neural networks for well log analysis. *International Journal of Coal Geology*. 2017. Vol. 181, p. 11-22. DOI: 10.1016/j.coal.2017.08.003
38. Guo Q., Ye M., Yang W.Q., Liu Z.M. A machine learning approach for electrical capacitance tomography measurement of gas-solid fluidized beds. *Aiche Journal*. 2019. Vol. 65. Iss. 6. DOI: 10.1002/aic.16583
39. Wen Z., Zhou C., Pan J. et al. Deep learning-based ash content prediction of coal flotation concentrate using convolutional neural network. *Minerals Engineering*. 2021. Vol. 174. N 107251. DOI:10.1016/j.mineng.2021.107251
40. Xu L., Cheng Y., Yin R., Zhang Q. Comparative study of regression modeling methods for online coal calorific value prediction from flame radiation features. *Fuel*. 2015. Vol. 142. P. 164-72. DOI: 10.1016/j.fuel.2014.10.081
41. Clauset A., Shalizi C.R., Newman M.E.J. Power-law distributions in empirical data. *SIAM Review*. 2009. Vol. 51, p. 661-703. DOI: 10.1137/070710111
42. Armaghani D.J., Hajihassani M., Bejarbaneh B.Y. et al. Indirect measure of shale shear strength parameters by means of rock index tests through an optimized artificial neural network. *Measurement*. 2014. Vol. 55, p. 487-498. DOI: 10.1016/j.measurement.2014.06.001
43. Neupane G., Donahoe R.J. Leachability of elements in alkaline and acidic coal fly ash samples during batch and column leaching tests. *Fuel*. 2013. Vol. 104, p. 758-770. DOI: 10.1016/j.fuel.2012.06.013
44. Abdi H., Williams L.J. Principal component analysis. *Wiley Interdisciplinary Reviews Computational Statistics*. 2010. Vol. 2. Iss. 4, p. 433-459. DOI: 10.1002/wics.101

***Authors*: Jinzhan Huang,** *Master of Engineering in Mineral Processing, https://orcid.org/0000-0003-2531-4834* (*China University of Mining & Technology, Xuzhou, China*), **Zhiqiang Li,** *Doctor of Engineering in Mineral Processing, https://orcid.org/0000-0002-3661-6443* (*China University of Mining & Technology, Xuzhou, China*), **Biao Chen,** *Master of Information and Communication Engineering, https://orcid.org/0000-0002-9304-6037* (*China University of Mining & Technology, Xuzhou, China*), **Sen Cui,** *Master of Information and Communication Engineering, https://orcid.org/0000-0003-3250-5292* (*China University of Mining & Technology, Xuzhou, China*), **Zhaolin Lu,** *Doctor of Computer Science, Associate Professor, https://orcid.org/0000-0002-9251-0758* (*China University of Mining & Technology, Xuzhou, China*), **Wei Dai,** *Doctor of Control Engineering, Professor, https://orcid.org/0000-0003-3057-7225* (*China University of Mining & Technology, Xuzhou, China*), **Yuemin Zhao,** *Doctor of Engineering in Mineral Processing, Professor, https://orcid.org/0000-0003-2848-5962* (*China University of Mining & Technology, Xuzhou, China*), **Chenlong Duan,** *Doctor of Engineering in Mineral Processing, Professor, https://orcid.org/0000-0002-8093-6719* (*China University of Mining & Technology, Xuzhou, China*), **Liang Dong,** *Doctor of Engineering in Mineral Processing, Professor, dongliang@cumt.edu.cn, https://orcid.org/0000-0003-0264-8807* (*China University of Mining & Technology, Xuzhou, China*).

The authors declare no conflict of interests.